PHILOSOPHICAL TRANSACTIONS A

royalsocietypublishing.org/journal/rsta

Research

Cite this article: Cooley S, Yang H, Virgin LN. 2023 3D-printing and cylinder buckling: challenges and opportunities. *Phil. Trans. R. Soc. A* **381**: 20220035.
https://doi.org/10.1098/rsta.2022.0035

Received: 2 September 2022
Accepted: 23 November 2022

One contribution of 13 to a theme issue 'Probing and dynamics of shock sensitive shells'.

Subject Areas:
civil engineering, structural engineering, mechanics

Keywords:
buckling, 3D-printing, experimental mechanics

Author for correspondence:
L. N. Virgin
e-mail: l.virgin@duke.edu

Electronic supplementary material is available online at https://doi.org/10.6084/m9.figshare.c.6373251.

THE ROYAL SOCIETY PUBLISHING

3D-printing and cylinder buckling: challenges and opportunities

S.A. Cooley[1], H. Yang[2] and L. N. Virgin[1]

[1]Department of Mechanical Engineering, Duke University, Durham, NC 27708, USA
[2]Department of Mechanical Engineering, University of Wisconsin, Madison, WI 53706, USA

LNV, 0000-0001-5990-0722

Cylinder buckling is notoriously sensitive to small geometric imperfections. This is an underlying motivation for the use of knock-down factors in the design process, especially in circumstances in which minimum weight is a key design goal, an approach well-established at NASA, for example. Not only does this provide challenges in the practical design of this commonly occurring structural load-bearing configuration, but also in the carefully controlled laboratory setting. The recent development of 3D-printing (additive manufacturing) provides an appealing experimental platform for conducting relatively high-fidelity experiments on the buckling of cylinders. However, in addition to geometric precision, there are a number of shortcomings with this approach, and this article seeks to describe the challenges and opportunities associated with the use of 3D-printing in cylinder buckling in general, and probing the robustness of equilibrium configurations in particular.

This article is part of the theme issue 'Probing and dynamics of shock sensitive shells'.

1. Introduction

Given the ubiquity of 3D-printing technology and the ability to produce geometrically non-simple objects with relatively high precision, it seems reasonable to assess the use of additive manufacturing (3D-printing) in the context of experimental cylinder buckling. Interest in this area has received recent impetus based on the notion of *probing* a structural system, especially one that is imperfection-sensitive.

This study is wholly experimental, and the paper discusses some of the main issues in the testing of axially loaded, 3D-printed cylindrical shells, emphasizing the advantages and disadvantages of this approach on a practical level.

(a) 3D-printing of slender structural elements

3D-printing has become increasingly sophisticated in recent years. The ability to produce geometrically precise physical objects is now a standard component in mechanical design. More recently, with improved resolution it is becoming possible to produce *slender* 3D-printed objects that possess a certain degree of flexibility [1,2], and this brings with it an opportunity to conduct experiments on elastically deformable structures which would otherwise be very difficult or impossible [3].

Cylinder buckling has a long history [4–13]. Many previous experimental studies in cylinder buckling have either focused on a single specific configuration based on a high-quality manufactured specimen, or repeated tests on soda cans. The latter has the advantage of high similarity between specimens and low cost, but a limited range of geometry. Also, with aluminium soda cans, a specimen often enters the range of plastic deformation under buckling conditions, and typically this means that buckling results in the destruction of the specimen. Research has particularly focused on the robustness of the buckling estimates of axially loaded cylinders and the role of initial geometric imperfections [14–21].

3D-printing now has access to a wide variety of materials. The most popular materials are a range of thermoplastics with acrylonitrile butadiene (ABS) and polylactic acid (PLA) being the most common. There are a number of subtleties involved in the 3D-printing process including infill percentage (which affects density) and print orientation (which can produce a little anisotropy) [1]. Furthermore, although these materials generally have an accessible elastic range (depending on geometry), their Young's modulus tends to be not as well defined as metals, they may exhibit a certain brittleness and even a little viscoelastic behaviour. This paper describes the use of 3D-printed cylinders in preliminary buckling studies. Despite some limitations, it is the sheer versatility of producing 3D-printed specimens, where the cylinder length, radius and thickness are all under the control of the experimentalist, that makes this approach worthy of consideration. And specimens that are nominally identical can be produced, opening the door to repeat testing and statistical evaluation. Perhaps the most appealing aspect of this approach is that cylinders can be produced with almost any form of geometric imperfection [22], from a number of sine waves in both longitudinal and circumferential directions to frustra to localized dimples. The cylinders described in this paper are produced to fit the range of 'practical' geometry, for example, in which the length-to-radius ratio is in the range 2–4, and the radius-to-thickness ratio is typically in the range of 100–150. The practical limitations associated with geometry (in actual size) will be described later.

(b) Probing and perturbing a structural configuration

When a cylinder buckles it is not only challenging to predict the buckling load, but also the shape it buckles into. And on subsequent compression a cylinder may switch between buckled shapes, including the appearance of hysteresis on unloading.

It is not uncommon for post-buckled structures (in general) to possess multiple equilibrium configurations. For example, a Euler strut, when loaded axially, will buckle in a preferred direction, depending on any inevitable bias in the nominally symmetric unloaded system. However, in addition to whatever natural load-path it follows, it is often possible to perturb the system into an alternative (near mirror-image) shape: a complementary equilibrium solution. Sometimes, under the gradual change of a control parameter, a system will suddenly snap between equilibrium configurations. That is, a limit point (saddle-node) bifurcation is encountered on the path. However, under a fixed value of the control, it is plausible to 'probe' the system, in order to explore possible adjacent configurations and possibly use the information

gained at various levels of axial loading to be able to predict load-carrying capacity. Clearly, there are a variety of ways of achieving this probing, a means of exploring the global potential energy landscape, including a suddenly applied (dynamic) disturbance [23], sometimes referred to as shock sensitivity [24], or a gradually applied lateral force. The latter is one of the motivations for the current study. Also, because we are typically dealing with high-dimensional systems a lateral, point probing force necessarily only explores a relatively restricted subset of the configuration space: the probing described in this paper only provides limited information, but shows promise.

An abstract form of probing was presented in [25], in which the authors produced a smooth prescribed 2D-surface and then measured the force required to move a small ball as it was moved (pushed and pulled) along the curved surface (in a gravitational field). Turning points corresponded to positions of equilibrium, with saddle-points playing a key role in organizing global features and basins of attraction. Integration of the force field was achieved from the force measurements and was used to reconstruct the surface contours.

The notion of lateral probing and its application to the buckling of cylindrical and spherical shells was developed by Thompson and co-workers [26,27]. Prior work involving non-destructive evaluation can also be found in [10,18]. Some experimental verification was conducted by Virot *et al.* [28] based on the testing of multiple aluminium soda cans. The current study exploits 3D-printing along the same lines but with added benefit of user-defined geometry.

Highly imperfection-sensitivity structures, like the cylindrical shell, are the focus of the current study [29]. The lateral probing of structures that possess multiple equilibrium configurations has been explored experimentally [30,31]. A typical example is a clamped, buckled rectangular plate. Under sufficient lateral point force the system can snap-through to the 'other-side'. This depends on the extent of buckling (which may be thermally induced [30]), material properties and geometry such as the panel thickness and aspect ratio. The path followed by the system under the action of a unidirectional probe depends on subtle features of the potential energy landscape [32], but the transition from one potential energy minimum to another remote one (including jumps) and the presence of unstable equilibria (saddle-points) is a key interest in this approach.

(c) Probing of axially loaded cylinders

Two aspects of cylinder buckling will be explored. First, a cylinder under moderate (pre-buckled) axial load will be subject to the probing of a small lateral point load. Figure 1*b* shows a schematic of a cylinder subject to axial load. If the system is load-controlled, for example, by adding weights to the top surface, the cylinder buckles (suddenly) with a rapid increase in axial deflection, often accompanied by plastic deformation. The buckling load is highly dependent on the initial imperfections. Initial probing is achieved by applying the small lateral force at relatively low levels of axial load in order to assess the robustness of the cylinder prior to buckling. That is, applying a steady perturbation to the side of the cylinder (point *a*) in order to assess the proximity of an unstable equilibrium (point *b*). Second, consider the situation described in figure 1*c*. Under conditions of displacement control, the system exhibits essentially the same initial buckling, but now the snap results in a sudden drop in the force. On subsequent end-shortening the system may display jumps between buckled shapes. At a fixed value of the end-shortening coexisting equilibrium shapes can also be subject to probing, for example, in going from point *a* to point *b*, presumably passing through an unstable equilibrium. If the system is then unloaded the cylinder snaps back to the original load-path marking the end of the region of hysteresis before returning to the unloaded (initial) configuration. This latter situation clearly requires the system to maintain elastic material behaviour during the loading, buckling and subsequent probing.

2. Geometry

In order to limit the range of parameters in this study, we specify what can be thought of as two baseline geometries and then explore the effect of changing a few parameters. In terms of nominal

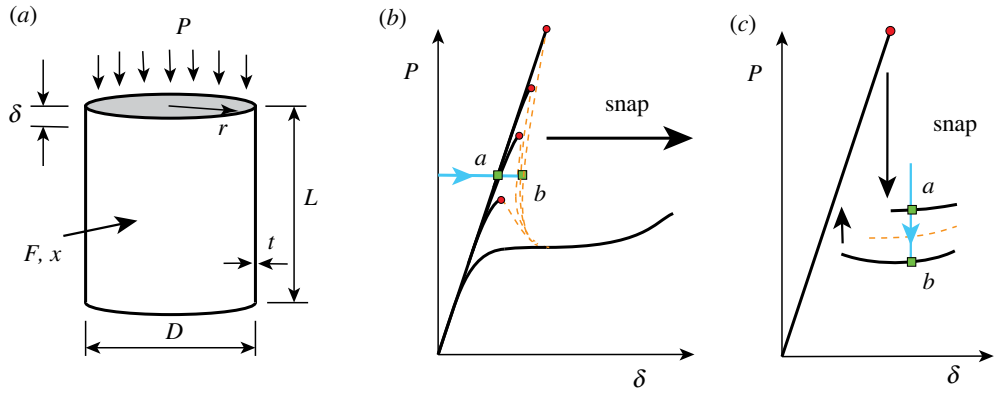

Figure 1. (*a*) The geometry of a cylinder, (*b*) axial load P versus axial deflection δ under force loading including the effect of initial imperfections and (*c*) coexisting post-buckled shapes and hysteresis under displacement loading. (Online version in colour.)

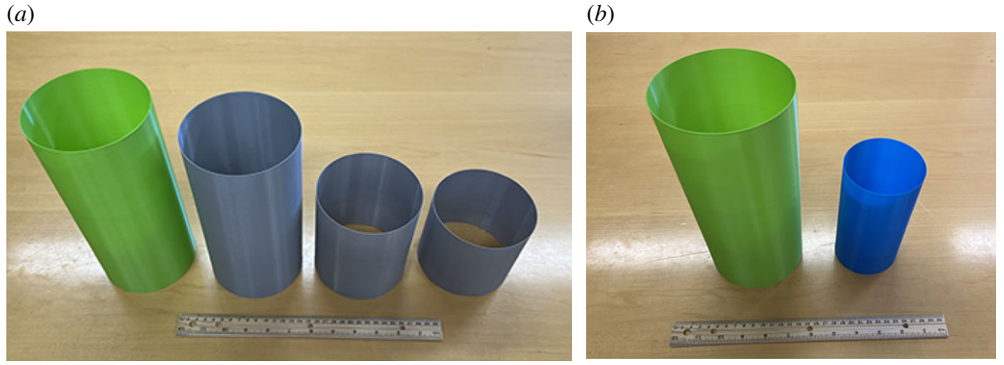

Figure 2. Some typical 3D-printed cylinders. (*a*) These four specimens all have a radius of $r = 57.5$ mm, thickness $h = 0.4$ mm, ($r/t = 137$) and the length $l = 250, 180, 130, 100$ mm (from left to right). (*b*) These two specimens have similar aspect ratios $l/r = 4.6$ and $l/r = 4.25$, respectively. (Online version in colour.)

cylinder sizing we start with fixing the radius $r = 57.5$ mm, length $L = 130$ mm, and then using the following printing approach:

— Nominal 0.8 mm thickness, using ABS thermoplastic (Stratsys Fortus)
— Nominal 0.4 mm thickness, using PLA thermoplastic (Ultimaker Cura)

ABS thermoplastic has a Young's modulus $E \approx 2.1$ GPa, and Poisson's ratio $\mu = 0.38$, and the Young's modulus for PLA is typically taken as 3.5 GPa, with a similar Poisson's ratio to ABS. We thus initially focus on the aspect ratios $L/r \approx 3$ and $r/h \approx 150$. Some typical specimens are shown in figure 2.

In order to achieve a *thin-walled* configuration within the realm of elastic behaviour, and given the limitations of a 3D-printer (build volume and nozzle size), a minimum wall thickness of $h = 0.4$ mm was the smallest dimension possible. Some of the results to be described later correspond to a wall thickness of approximately 0.8 mm, and we shall see that this typically resulted in the material exceeding its yield stress at buckling, which for ABS is typically in the vicinity of 30–50 MPa. It is interesting to note that this kind of thermoplastic exhibits a little localized discolouration if over-stressed, and leaves a distinct impression of the buckling shape as a plastic region is encountered.

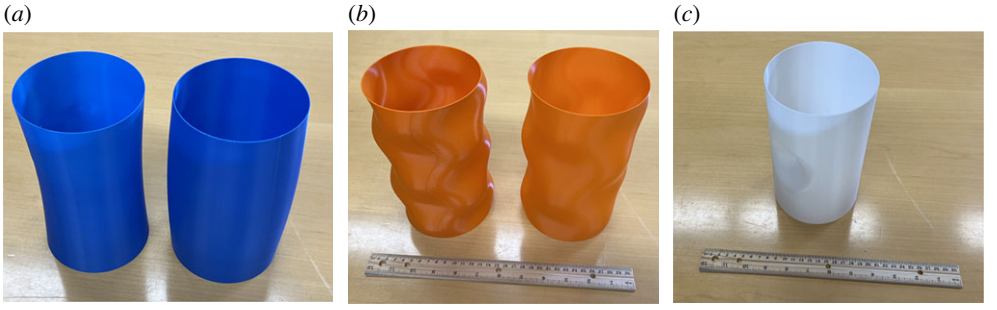

Figure 3. Cylinders with 'non-perfect' geometry. (*a*) Two cylinders with a single half-sine wave in the longitudinal direction, (*b*) Two cylinders with multiple sine waves in the longitudinal and circumferential directions and (*c*) a cylinder with a single localized dimple. (Online version in colour.)

The length was varied from $L = 100$ to 200 mm, and a few tests were conducted on cylinders printed with PLA thermoplastic.

The boundary conditions consisted of shallow V-grooves machined in aluminium end-plates, providing minimal resistance to rotation and approximating a pinned, or shear diaphragm, edge condition. As mentioned earlier, the 3D-printing process easily handles the incorporation of stiff end-plates for clamped boundary conditions [33], which we shall return to later. Since the end-plattens involved machining aluminium plates, it was easier to change the length of the cylinders (rather than the radius), and even though it was anticipated that this parameter would have minimal effect on buckling it did provide additional testing opportunities.

Most cylinders were printed in a nominal 'pristine' geometry, although (of course) inevitable initial imperfections were unavoidable, including the challenge in ensuring that the axial load was applied evenly at both ends of the cylinder. However, a number of designed deviations from the perfect geometry were also implemented. Figure 3 shows some of these initial shapes. Figure 3*a* shows cylinders in which there is a mild half-sine wave in the longitudinal direction (inwards and outwards, the latter barrel-like). Figure 3*b* shows cylinders in which an integer number of complete half-sine waves are printed in the longitudinal and circumferential directions. Figure 3*c* shows a cylinder printed with a single, localized 'dimple', representative of damage. In figure 3*b*,*c* the magnitude of the deviations from a pure cylinder are exaggerated for illustrative purposes. Only results from the pristine and the barrel-like geometries are included in this paper, with the other geometries mentioned to convey the sheer versatility of 3D-printing and the potential for assessing the role played by specific geometric forms in the future.

Considerable effort was put into printing cylinders with as thin a cross-section (wall thickness) as possible. Some of the results to be described involve a wall thickness of 0.8 mm. Buckling load tests typically resulted in destruction of the specimens. However, results will be described for initial stiffness, buckling load and pre-buckling probing. A slicing technique called 'vase mode' was then found to print cylinders with a thickness of 0.4 mm, with the same overall dimensions.

The *gcode* files for these particular cylinders were generated using the 'spiralize outer contour' experimental mode in Ultimaker Cura. In practice, the nozzle extrudes filament in a continuous spiral motion along the contour of the shape to generate a one-walled 'vase'. Unless modified to perform otherwise, the object will have a wall thickness t equal to the nozzle diameter—in this case, 0.4 mm. These specimens were amenable to repeated (elastic) testing through post-buckling. There was some small notable degradation when these cylinders were tested more than a few times. Results for the thinner wall thickness cylinders are detailed later for post-buckled probing.

Both ABS and PLA material were used. The latter possesses a little higher Young's modulus [1], so we would expect a corresponding increase in stiffness and buckling resistance, although, due to the printing process, the precise value of Young's modulus is not as invariant as aluminium, for example.

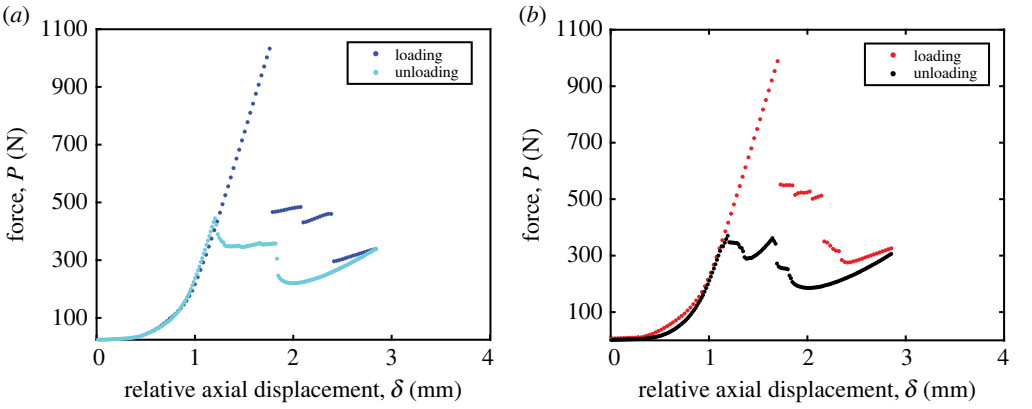

Figure 4. Axially loading of a typical cylinder. (*a*) Initial testing through loading and unloading and (*b*) the same cylinder subject to a second test. (Online version in colour.)

The measuring methods are not especially sophisticated, with emphasis placed on qualitative behaviour. For example, there is an issue with establishing an appropriate datum for axial deformation, since the ends need to 'bed' into the V-grooves. However, tests were consistent, for example, the rate of loading was maintained at 1 mm per minute. Two different universal testing machines were used: Test Resources 830LE-A (with a 50 kN load cell), and Lloyds Instruments LRX Plus (with a 5 kN load cell).

3. Conventional buckling—initial buckling results

We initially focus on cylinders printed with PLA and the following dimensions: $L = 150$ mm; $r = 57.5$ mm and $t = 0.4$ mm. Figure 4*a* shows the axial loading of a typical cylinder. After an initial settling of the boundary conditions the axial deflection of the cylinder proceeds at a constant rate with a proportionally corresponding load-reading. The slope under increasing end-shortening (the dark blue data points) is approximately 1150 N mm^{-1} and buckling occurs at a little over 1 kN. Immediately after buckling the load drops to about 470 N with further drops as the buckling shape suddenly shifts. There is a gradual increase in the load as the cylinder experiences considerable buckling deflection. The end-shortening is then reversed (the light blue data points) and the cylinder proceeds to return to its unbuckled shape, following different path(s), rejoining the initial linear behaviour and ultimately the original state. The same cylinder was then retested and the results shown in figure 4*b*. The behaviour is very similar, apart from small differences in the post-buckled behaviour. This post-buckled jumping between shapes was first identified by Yamaki [6], and also found in [29,34]. A recent example of following multiple paths can be found in [35], based on sophisticated numerical analysis.

The classic buckling load for an axially compressed simply supported thin cylinder is [36]

$$P_{\rm cr} = \frac{EA(t/r)}{\sqrt{3(1-\nu^2)}} = \frac{2\pi Et^2}{\sqrt{3(1-\nu^2)}}. \tag{3.1}$$

For a typical set of printed cylinders we have $E = 2.1$ GPa (ABS); $t = 0.77$ mm; $\nu = 0.38$ (Poisson's ratio), which gives $P_{\rm cr} = 4.883$ kN, and corresponding to $r/t = 75$. Approximately 10 cylinders were printed with a mean buckling load of approximately 3 kN. The second set of cylinders were printed with $E = 3.5$ GPa (PLA); $t = 0.42$ mm; $\nu = 0.38$, which gives $P_{\rm cr} = 2.421$ kN, and corresponding to $r/t = 137$. Approximately 30 cylinders were printed with a mean buckling load of 1 kN (the

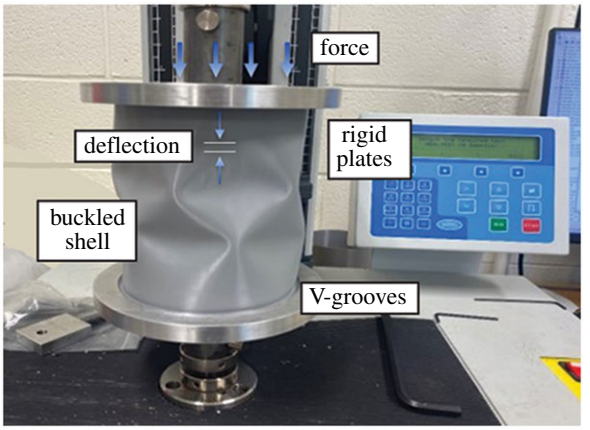

Figure 5. A typical buckled shape under a fixed end-shortening. The material in this case exceeded its yield, leaving mild but regularly patterned discolouration on load removal. (Online version in colour.)

cylinder in figure 4 was representative). As expected the classical theory grossly over-estimates the buckling capacity. The knock-down factor (KDF) formula commonly adopted [7,9,37–39]

$$\frac{P_{\text{exp}}}{P_{\text{cr}}} = 1 - 0.901\left[1 - \text{e}^{-1/16\sqrt{r/t}}\right] \tag{3.2}$$

suggests a lower bound value of about $P_{\text{exp}}/P_{\text{cr}} \approx 0.62$ for the first set of cylinders and about 0.53 for the second set of cylinders. A few other cylinders were printed, for example with thickness between the two sets (≈0.5–0.6 mm), and these buckled in an intermediate range of loads and corresponding KDFs.

This geometry corresponds to another commonly used non-dimensional parameter: the Batdorf number, i.e. $Z = L^2\sqrt{1-\mu^2}/(rt)$ [5], and for the printed cylinders in the current study we obtain geometry in the range $Z = 350 \rightarrow 1500$. We also note that alternative approaches to KDFs can be found in [14–16,18].

The thinner cylinders tolerated quite large deflections into the post-buckled range and regained their original configuration upon the removal of the axial load. This elastic behaviour paved the way for repeat testing. In the past Mylar has proved to be a useful elastic material for cylinder buckling experiments, although it cannot produce a prescribed form of initial geometric imperfection that 3D-printing facilitates [10,11].

Figure 4*a* shows typical measured post-buckling characteristics. Immediately after buckling, under constant displacement control, the load drops by approximately 50%. On subsequent end-shortening, there occur a number of mode jumps in the buckled shape. A relatively heavily buckled shape is shown in figure 5. On the reversal of the end-shortening the cylinder unbuckles along different paths before returning to its initial pristine shape. Very similar behaviour is observed in the repeat testing of the same cylinder (see figure 4*b*).

4. Probing

(a) Probing the pre-buckling equilibrium

Preliminary probing tests were conducted on cylinders with nominal dimensions 0.8 mm thickness, radius 58 mm and length 200 mm, that is, the dimensions passed to the 3D-printer. Direct measurements gave $t = 0.77$ mm and $r = 57.5$ mm. The general test configuration is shown in figure 6.

Figure 7*a* shows a typical axial-force versus deflection relation, in which a buckling load of close to 3 kN was observed. The sudden snap at buckling was often an initiator of damage. The

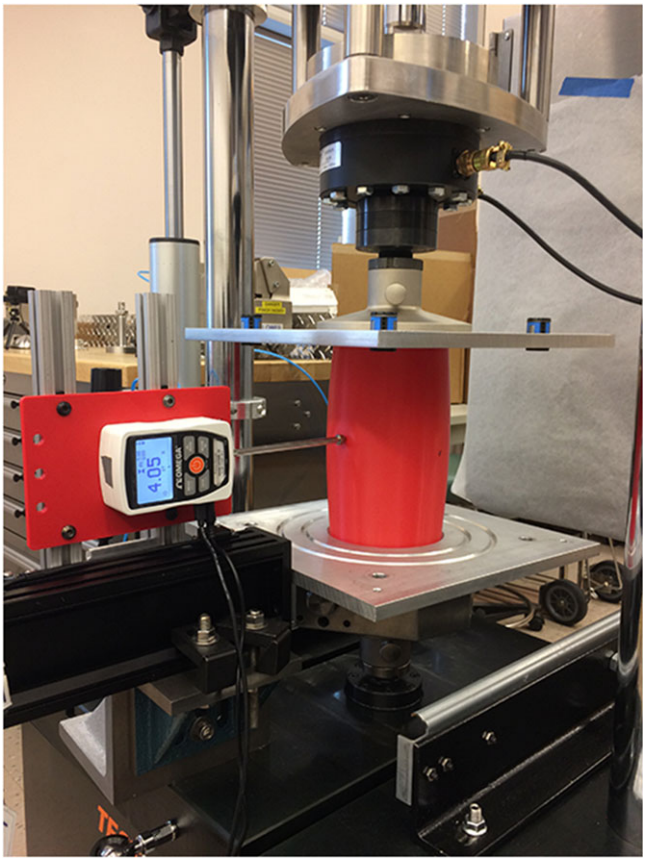

Figure 6. A cylinder in its testing configuration. The cylinder is subject to a fixed axial displacement, where it is probed. The probing force and corresponding deflection are recorded. (Online version in colour.)

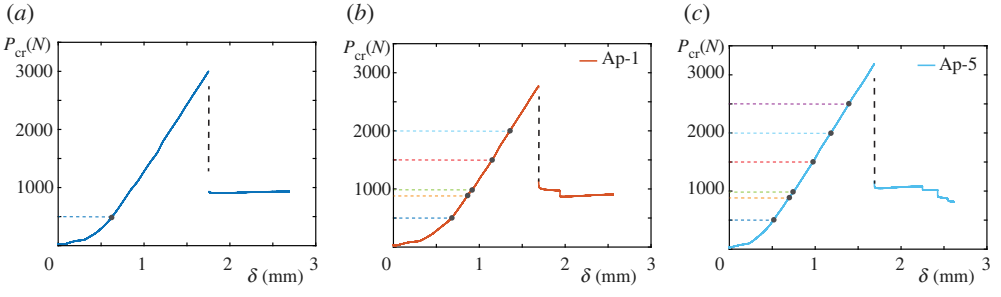

Figure 7. Axial load versus axial deflection. (*a*) The pristine cylinder, (*b*) a barrel-like cylinder with a sine wave amplitude of 1 mm over a length of 200 mm and (*c*) a barrel-like cylinder with a sine wave amplitude of 5 mm over a length of 200 mm. (Online version in colour.)

results shown in figure 7*b*,*c* correspond to cylinders that were printed with slight longitudinal outward curvature (see figure 3*a*): for the cylinder in figure 7*b* the central amplitude is 1 mm, and 5 mm in figure 7*c*, in which the longitudinal shape consisted of a half-sine wave.

Each of these cylinders were then subject to lateral probing. The probing force was measured using a digital load cell (Omega DFG35-10, with a 50 N capacity and 0.05 N resolution), and probe position measured using the linear transducer (Bislide by Velmex moving at a rate of

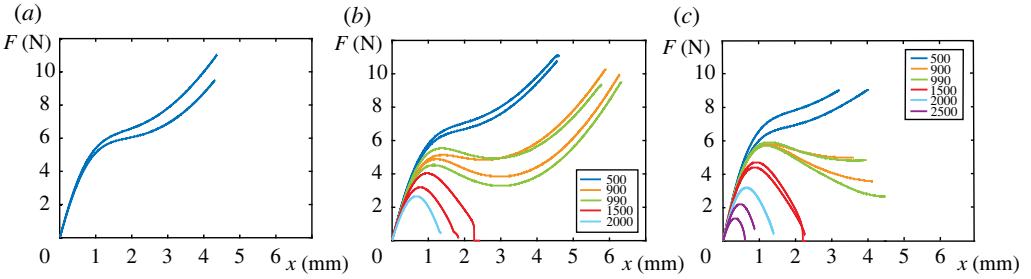

Figure 8. Probing of the cylinders from this figure. (*a*) Pristine cylinder, (*b*) Small-amplitude barrel-like shape and (*c*) larger amplitude barrel-like shape. (Online version in colour.)

0.0127 mm s^{-1}). The probing results are shown in figure 8, corresponding to the axial loading cases shown in figure 7. The procedure was as follows. The testing machine loaded the pristine (figure 8*a*) cylinder to 500 N. The lateral probe was then applied giving the load–deflection (F versus x) relation shown. This was repeated twice. However, this geometry resulted in cracking of the specimen when the axial load was subsequently increased. In figure 8*b*, the cylinder was probed at axial loads corresponding to approximately 17%, 30%, 33%, 50% and 67% of the buckling load. The changing nature of the probe load–deflection relation is apparent, and the dropping to zero of the probe load precipitated the loss of stability for the cases in which the applied axial load was closer to buckling. This has been observed in previous studies [28]. The results of the more barrel-like cylinder are shown in figure 8*c*. It is important to state that the results shown here illustrate the most consistent results of the many cylinders that were tested. A problem with these (relatively thicker) cylinders was that they often broke during testing. As mentioned earlier, considerable effort was then placed on producing 3D-printed cylinders with as thin a wall thickness as possible.

(b) Probing the post-buckling equilibria

In addition to probing the pre-buckled cylinder, with a view to assessing the proximity of unstable behaviour, we can also use a form of probing to explore some of the characteristics of the post-buckled behaviour [30,31,40]. The following results correspond to cylinders that were printed with nominal 0.4 mm thickness, which we already seen generally provides a greater range of elastic behaviour, and using PLA with $r = 57.5$ mm, $L = 150$ mm. We first describe a preliminary study in which a cylinder is buckled, and then held under fixed conditions in that buckled configuration. A 'probe' (in this case a simple pencil with end-eraser) is manually pushed onto the side of the cylinder, at approximately mid-height, and where a buckled shape is pointed outward (locally). An illustration is shown in figure 9*a* plotting axial load versus axial displacement in the usual manner. In figure 9*b* of this figure is shown the shape at point A in figure 9*a*, corresponding to $P \approx 450$ N and $x \approx 2$ mm, which is then pushed through to an adjacent coexisting shape at the same point displacement but now corresponding to a load of $P \approx 280$ N, point B. The limitation of a single point force only provides a very limited path through the (high-dimensional) potential energy landscape [32,41], but this approach has been shown to work well in low-order beams and arches [42–44]. There are challenges with the subtleties of the probe application. For example, the profile of the probe tip, and whether to fix the probe tip to the surface of the cylinder (thus allowing pulling as well as pushing), and possibly inhibiting rotation.

The experimental probing system was then implemented based on a more systematic approach. The linear displacement transducer and digital load cell were again set-up to record lateral probing. A similar cylinder to the preliminary study was printed and the test results shown in figure 10. The axial loading and unloading are shown in figure 10*a*. This time the cylinder buckles at a somewhat lower load: 870 N, and again undergoes some shape changing

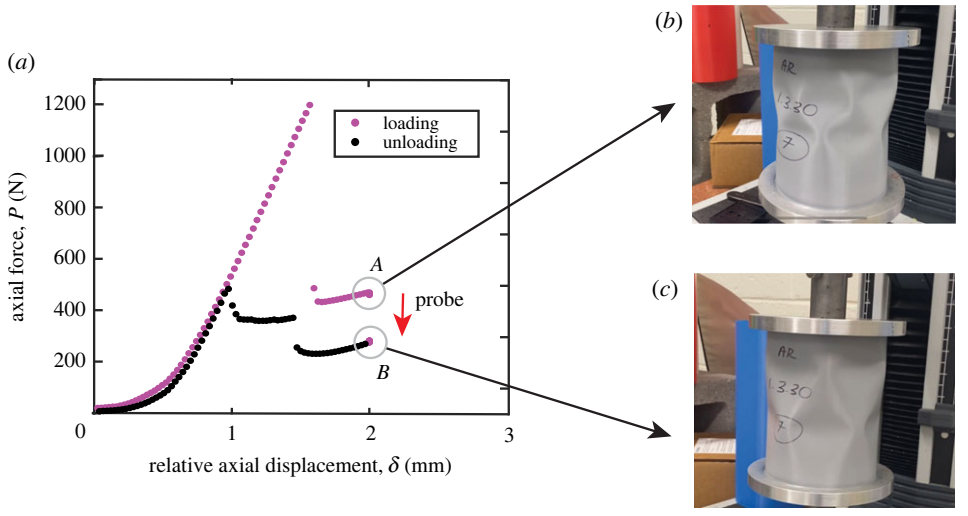

Figure 9. (*a*) The force–deflection behaviour extending to post-buckling, (*b*) the pre-probing buckled shape and (*c*) the shape the cylinder snaps to after probing. (Online version in colour.)

on subsequent loading. When the compression has reached a displacement of close to 2 mm, corresponding to a measured axial load of ≈410 N, the axial compression is held fixed at that value (labelled *A*). The probe is then used to push on an outward 'dimple', causing the cylinder to change shape. The 'before' and 'after' images are shown in figure 10*c*,*d*. The relation between the probe force and its displacement are shown in figure 10*b*. On initial engagement of the probe tip there is a rapid increase in displacement, until the force reaches ≈6 N followed by a drop in load as a new dimple under the probe tip begins to form. Under further probing the force recovers and again reaches a level of ≈6 N, at which point the shapes suddenly changes again, via a snapping motion, before the probe loses contact at a probe displacement of ≈9 mm (and a load of zero). This alternate equilibrium configuration is indicted by the point *B* in figure 10*a*,*b*. The probe then 'catches-up' with the surface of the cylinder again and gradually pushes on the new shape. Under axial load removal the cylinder shape(s) then follows the path indicated in figure 10*a*, rising to a maximum load of ≈392 N before returning to the unloaded 'pristine' shape. Clearly, there are a myriad of ways of probing, or perturbing, an equilibrium configuration, and a number of coexisting shapes are possible. The potential energy landscape that is being traversed is high-dimensional, and the current study describes a very specific probing that gives some insight but to only a limited extent.

5. Discussion and future directions

3D-printing continues to improve in terms of accuracy, resolution and material properties, not to mention cost. In this study, we have seen that the slenderness of structural components is limited by the overall print area, but also the minimum (thickness) dimension that can be printed. The minimum available thickness is not only important in terms of representing practical slender (scaled) cylinder geometry, but also in terms of managing stress in order to avoid material failure.

While general shape can be easily controlled through 3D-printing, there still exists limitations to projecting print accuracy. Vase mode, for example, generates cylinder wall thickness according to nozzle diameter, meaning smaller nozzles (e.g. 0.25 mm) produce even more slender shells. Attempting wall thicknesses different from the nozzle's diameter, however, can amplify print variation. The user may increase bed temperature and filament flow to achieve higher thicknesses, but should expect stringing and other deformities. The authors found 0.6 mm to be the practical limit for a 0.4 mm nozzle. Furthermore, vase mode commonly introduces a 3D-printing issue

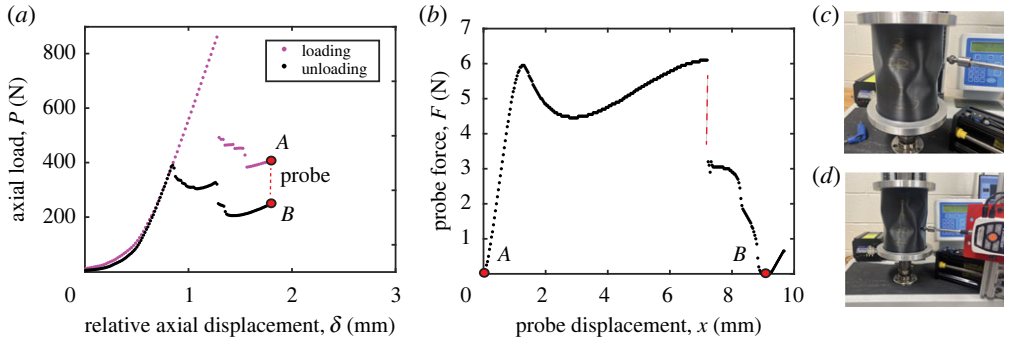

Figure 10. The post-buckled experimental probing configuration. (*a*) Axial load versus axial displacement, (*b*) probe force–deflection relation and (*c*) pre-probing post-buckled shape and (*d*) alternate coexisting post-buckled shape after probing. (Online version in colour.)

known as 'elephant's foot', i.e. a small splaying out where the thermoplastic is first laid down on the printer plate. It can be thought of as the gentle sinking of the print's initial layers. Elephant's foot can be reduced through regular printer maintenance, slower print speeds and sufficient cooling. Even so, the authors observed it cannot be totally removed without manual methods (which were not explored in this study). There was no clear effect of the orientation (i.e. contact on top or bottom platten) of the elephant's foot on the critical buckling load, but it seems to be partly responsible for the nonlinear stiffness effect during the early stages of axial loading.

The results presented so far corresponded to boundary conditions based on a simple V-groove routed in the aluminium end-plates using a CNC milling machine. There are minor issues related to the seating of the edge of the cylinder into the V-groove. The V-grooves incorporated a small flat in the corner of the groove of roughly the same width as the cylinder thickness. Although edge rotation in the radial direction did not appear to be influenced, this may partly explain the initial nonlinear stiffness in the typical force–deflection relation. In order to shed light on the 'simply supported' boundary condition consider the data supplied in figure 11. Here, we compare the axial loading for three different cases: V-grooves at both ends; flat surfaces at both ends; and mixed, i.e. a V-groove at one end and a flat surface at the other. In this plot, the data has been shifted so that the slopes match in order to highlight the difference in the initial engagement in the early stages of loading. It can be seen that the boundary condition has a minor effect on the initial nonlinearity. But each relation shows the initial nonlinearity, suggesting that the loading plates are probably more responsible for this behaviour in addition to some localized material properties. The difference in the critical buckling load and post-buckled behaviour is likely to do with general imperfection effects rather than boundary conditions, *per se*, this effect should not have much influence on probing under moderate or higher levels of axial loading.

Given the versatility of 3D-printing, it is feasible to print integral relatively thick end-plates to provide effectively clamped boundary conditions. An example of such a print is shown in figure 12, in which it is a simple matter to change the dimensions of the thick end, even to the extent of integrally printing thick solid plates. The rounding-off of interior corners (filleting) is a convenient means of reducing stress concentrations. 3D-printing a cylinder with a thick end ring to mimic a clamped boundary condition but with the other end simply supported, led to an increase in the buckling load (all other things held constant), but is not specifically reported here.

The tests described in this paper correspond to cylinders printed with either PLA or ABS thermoplastic. Typical values of Young's modulus are 3.5 GPa for the former, and 2.1 GPa for the latter. Most of the 0.8 mm thick cylinders were made of ABS, and the 0.4 mm thick cylinders made of PLA. These thermoplastics can be somewhat brittle, and avoiding yield was the main motivation for producing as thin a cylinder as possible. A little anisotropic behaviour has been

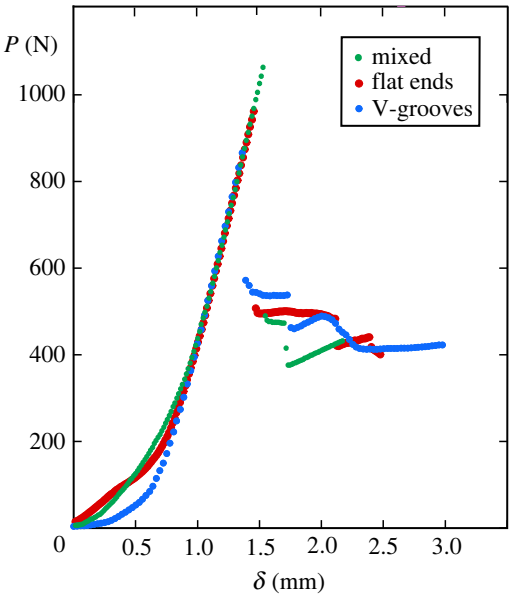

Figure 11. Effect of the 'simple-support', comparing the effect of flat loading surfaces and V-grooves. (Online version in colour.)

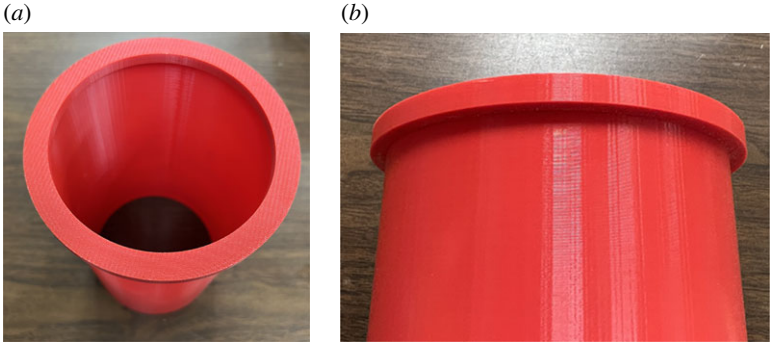

Figure 12. (*a*,*b*)Cylinders with a 'built-in' end perimeter. The junction between the cylinder ends and the thick support can be enhanced with fillets to reduce stress concentrations. (Online version in colour.)

observed in some flexural 3D-printed elements [1], but the axi-symmetric nature of printing cylinders (in a vertical orientation) largely eliminated this effect.

Thermoplastics have a tendency to be somewhat sensitive to temperature changes, and creep can be an issue for systems undergoing elevated stresses for extended periods of time. The authors considered how material creep may affect the delay between loading and unloading tests on a given cylindrical shell. Typically, a 0.4 mm shell compression test was extended 1–1.5 mm beyond its buckling point, then was paused for approximately one minute while the setup was adjusted to begin unloading. To ensure material weakening was not a concern, a typical cylinder ($L/r \approx 3.2$) was loaded to 900 N then held for over 20 min. The monitored load did not decrease appreciably during this period, but rather fluctuated by at most a few Newtons. However, an example of viscoelastic behaviour is shown in figure 13 during a probing test. In this case, a cylinder is compressed under displacement control to a level of $P = 800$ N, as shown in figure 13*a*. The probe load cell is then pushed at a location mid-length, and corresponding to $F = 3.4$ N. Under nominally fixed conditions the probe load slowly reduces such that the load cell displays a

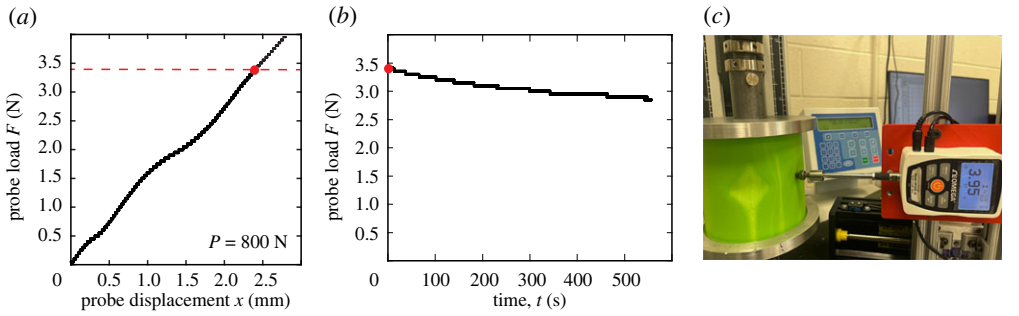

Figure 13. An example of mild viscoelasticity. (*a*) A typical lateral probing behaviour under a fixed axial load of 800 N, (*b*) the gradual stress relaxation under constant axial displacement and (*c*) an image of the probe during creep testing (taken at a slightly higher probe force level than that shown in (*b*)). (Online version in colour.)

reading of about 3 N after 9 or 10 min. The 0.05 N resolution of the digital load cell is apparent in the non-smooth nature of the data in figure 13*b*. Recent developments in additive manufacturing have included using more elastic materials, partly to avoid viscoelastic behaviour.

Figure 3 showed the relative ease with which subtle geometric deviations can be printed into the cylinder. Seeding initial imperfections in this way, can facilitate certain types of buckling, and especially exploiting localized 'dimples' has been discussed in the recent literature [15,16,18,19]. Producing accurately a cylinder of the type shown (exaggerated) in figure 3*b* for example, would be very challenging without the capabilities of 3D-printing.

The nature of the probing is subject to a high number of choices. For example, the placement and direction of the probe needs to be thoroughly explored. The initial probing involved a rubberized tip (a pencil), whereas the controlled probe caused a little sliding on the surface of the cylinder as the probe proceeded to press against the cylinder. This was also mitigated to a certain extent by coating the rounded rubber probe tip with epoxy anti-slip aerosol solution. If the probe tip is too sharp then a little localized plastic yielding can occur. Future development may explore the extent to which using multiple probes might provide more useful constraints in exploring the potential energy landscape [29,32]. A very recent publication also suggested using multiple probes in order to enhance the 'ridge-tracking' associated with probing [45], i.e. a (linear) correlation between the peak lateral probe load and the axial buckling load, useful for prediction purposes based on extrapolation. 3D-printing also has scope for producing shells of variable thickness [37,46,47], spherical shells [26,48], and the incorporation of stiffening ribs is straightforward [38,49].

Finally, the changing shape under load (both pre- and post-buckled) is an opportunity for digital image correlation (DIC). For example, the shapes shown in figure 9*b*,*c* were not specifically monitored in this study, although certain broad features of the shape were noted to provide confidence in the identification of distinct post-buckled shapes, for example to characterize shapes *A* and *B* in figures 9*a* and 10*a*, respectively. Dynamic DIC can be used to measure vibration, with its clear connection with stiffness [50,51], although this is not specific to 3D-printed specimens [50].

We summarize our general findings in terms of using 3D-printing in the context of cylinder buckling and probing.

Advantages:

— Since 3D-printing is based on data, cylinders can be produced over a comprehensive range of thin-walled geometries.
— Initial geometric imperfections can be routinely incorporated into the (essentially stress-free) printed shape, based on a mathematical prescription and even incorporating

random effects, for example where the prescribed undulations exhibit some specified variation.
— Boundary conditions, e.g.clamped ends, can be conveniently incorporated integrally within the print.
— Other geometric complexities can be easily added, e.g, longitudinal, circumferential and even helical stiffeners or cut-outs.
— Typically no seam or joins occur, and features such as filleting can be used to minimize stress concentrations.
— A single geometry can be repeat printed on the same machine, to the same precision, opening the possibility of conducting multiple tests (especially in identifying coexisting states) and assessing statistical properties.

Disadvantages (mostly concerning material properties):

— The typical materials used in 3D-printing (thermoplastics) possess the typical mechanical shortcomings of thermoplastics. For example, elastic flexural modulus, strength (yield stress) and density are all somewhat imprecise.
— In addition, second order material effects include a little viscolasticity (creep), brittleness and sensitivity to the thermal environment.

The material properties are properly viewed in comparison with metals, which typically have very precise Young's modulus, for example, and seldom suffer from creep. But new materials and higher resolution 3D-printers continue to improve, and the incorporation of composite materials is gaining traction.

6. Conclusion

Predicting the buckling load of an axially loaded cylinder, and the shape(s) it takes as buckling proceeds is challenging. 3D-printing shows promise in facilitating experimental studies in which there is considerable control over the geometry in general and the accuracy of reproducing a given geometry. 3D-printers that use metal, for example, titanium, are becoming more popular, and provide future opportunities given some of the material shortcomings of thermoplastics as outlined above. Probing can be achieved both prior to, and after, buckling, and this paper has presented some initial studies in which the opportunities and challenges of using 3D-printing in the context of cylinder buckling have been discussed.

Data accessibility. The data are provided in electronic supplementary material [52].

Authors' contributions. S.C.: data curation, investigation, methodology, resources, software, validation, visualization, writing—review and editing; H.Y.: data curation, investigation, methodology, software, validation, writing—review and editing; L.N.V.: conceptualization, data curation, funding acquisition, investigation, methodology, project administration, resources, supervision, visualization, writing—original draft.

All authors gave final approval for publication and agreed to be held accountable for the work performed therein.

Conflict of interest declaration. We declare we have no competing interests.

Funding. This research was supported with funding from the NSF (CMMI 1926672). The opinions, findings and conclusions or recommendations expressed are those of the author(s) and do not necessarily reflect the views of the National Science Foundation.

Acknowledgements. The authors are grateful to Yue Guan, of the University of Memphis, Michael Thompson of Cambridge University UK, Charles Cervi of Duke University and Giles Hunt of Bath University UK for helpful discussions.

References

1. Virgin LN. 2017 On the flexural stiffness of 3D printer thermoplastic. *Int. J. Mech. Eng. Educ.* **45**, 59–75. (doi:10.1177/0306419016674140)
2. Virgin LN. 2021 Simultaneous buckling, contact, and load-carrying capacity. *ASCE J. Eng. Mech.* **147**, 04021023. (doi:10.1061/(ASCE)EM.1943-7889.0001926)
3. Guan Y, Virgin LN, Helm D. 2018 Structural behavior of shallow geodesic lattice domes. *Int. J. Solids Struct.* **155**, 225–239. (doi:10.1016/j.ijsolstr.2018.07.022)
4. von Karman TV, Tsien HS. 1941 The buckling of thin cylindrical shells under axial compression. *J. Aerosol. Sci.* **8**, 303–312. (doi:10.2514/8.10722)
5. Batdorf SB. 1947 A simplified method of elastic-stability analysis for thin cylindrical shells. NACA Technical Report 874. Washington, DC: NACA.
6. Yamaki N. 1959 The post-buckling behaviour of rectangular plates with small initial curvature loaded in edge compression. *J. Appl. Mech.* **26**, 407–414. (doi:10.1115/1.4012053)
7. Seide P, Weingraten VI, Morgan EJ. 1960 The development of design criteria for elastic stability of thin shell structures. Technical Report STL/TR-60-0000-19425. Space Technologies Laboratories.
8. Horton WH, Durham SC. 1965 Imperfections, a main contributor to scatter in experimental values of buckling load. *Int. J. Solids Struct.* **1**, 59–72. (doi:10.1016/0020-7683(65)90015-6)
9. NASA. 1965 Buckling of thin-walled circular cylinders, NASA space vehicle design criteria. Technical Report Technical Report SP-8007. NASA.
10. Eßlinger M, Geier B. 1972 Egerechnete nachbeullasten als untere grenze der experimentallen axialen beullasten von kreiszylindern. *Der Stahlbau* **41**, 353–359.
11. Yamaki N 1984 *Elastic stability of circular cylindrical shells*, vol. 27. Applied Mathematics and Mechanics. Amsterdam, The Netherlands: Elsevier.
12. Croll JGA, Batista RC. 1981 Explicit lower bounds for the buckling of axially loaded cylinders. *Int. J. Mech. Sci.* **23**, 331–343. (doi:10.1016/0020-7403(81)90063-1)
13. Calladine C. 1983 *The theory of shell structures*. Cambridge, UK: Cambridge University Press.
14. Evkin A. 2015 Analytical model of local buckling of axially compressed cylindrical shells. *Thin-Walled Struct.* **168**, 108261. (doi:10.1016/j.tws.2021.108261)
15. Krasovsky V, Evkin A. 2021 Experimental investigation of buckling of dented cylindrical shells under axial compression. *Thin-Walled Struct.* **164**, 107869. (doi:10.1016/j.tws.2021.107869)
16. Wagner H, Hühne C, Niemann S, Khakimova R. 2017 Robust design criterion for axially loaded cylindrical shells—simulation and validation. *Thin-Walled Struct.* **115**, 154–162. (doi:10.1016/j.tws.2016.12.017)
17. Wagner H-N-R, Hühne C, Niemann S. 2020 Buckling of launch-vehicle cylinders under axial compression: a comparison of experimental and numerical knockdown factors. *Thin-Walled Struct.* **155**, 106931. (doi:10.1016/j.tws.2020.106931)
18. Hühne C, Rolfes R, Breitbach E, Teßmer J. 2008 Robust design criterion for axially loaded cylindrical shells—simulation and validation. *Thin-Walled Struct.* **46**, 947–962. (doi:10.1016/j.tws.2008.01.043)
19. Wang B, Hao P, Li G, Fang Y, Wang X, Zhang X. 2013 Determination of realistic worst imperfection for cylindrical shells using surrogate model. *Struct. Multidisc. Optim.* **48**, 777–794. (doi:10.1007/s00158-013-0922-9)
20. Lee A, Marthelot J, Lopez Jimenez F, Hutchinson JW, Reis PM. 2016 The geometric role of precisely engineered imperfections on the critical buckling load of spherical shells. *J. Appl. Mech.* **82**, 111005. (doi:10.1115/1.4034431)
21. Wang B, Du K, Hao P, Tian Y, Chao YJ, Jiang L, Xu S, Zhang X. 2019 Experimental validation of cylindrical shells under axial compression for improved knockdown factors. *Int. J. Solids Struct.* **164**, 37–51. (doi:10.1016/j.ijsolstr.2019.01.001)
22. Hu N, Burgueno R, 2015 Tailoring the elastic post-buckling response of cylindrical shells: a route for exploiting instabilities in materials and mechanical systems. *Extr. Mech. Lett.* **4**, 103–110. (doi:10.1016/j.eml.2015.05.003)
23. Hilburger MW, Waas AM, Starnes JH. 1997 Modeling the dynamic response and establishing post buckling snap-through equilibrium of discrete structures via a transient analysis. *J. Appl. Mech.* **64**, 590–595. (doi:10.1115/1.2788933)

24. Thompson JMT, Sieber J. 2016 Shock-sensitivity in shell-like structures: with simulations of spherical shell buckling. *Int. J. Bifurcat. Chaos* **26**, 1630003. (doi:10.1142/S0218127416300032)
25. Xu Y, Virgin LN. 2018 Probing the force field to identify potential energy. *J. Appl. Mech.* **86**, 101008. (doi:10.1115/1.4044305)
26. Hutchinson JW, Thompson JMT. 2017 Nonlinear buckling behaviour of spherical shells: barriers and symmetry-breaking dimples. *Phil. Trans. R. Soc. A* **375**, 20160154. (doi:10.1098/rsta.2016.0154)
27. Thompson JMT, Hutchinson JW, Sieber J. 2017 Probing shells against buckling: a non-destructive technique for laboratory testing. *Int. J. Bifurcat. Chaos* **27**, 1730048. (doi:10.1142/S0218127417300488)
28. Virot E, Schneider T, Rubinstein SM. 2017 Stability landscape in shell buckling. *Phys. Rev. Lett.* **119**, 224101. (doi:10.1103/PhysRevLett.119.224101)
29. Hunt GW, Lord G, Peletier M. 2003 Cylindrical shell buckling: a characterization of localization and periodicity. *Discrete Contin. Dyn. Syst. B* **3**, 505–518. (doi:10.3934/dcdsb.2003.3.505)
30. Ehrhardt DA, Virgin LN. 2019 Experiments on the thermal post-buckling of panels, including localized heating. *J. Sound Vib.* **439**, 300–309. (doi:10.1016/j.jsv.2018.08.043)
31. Ehrhardt DA, Virgin LN, Spottswood SM. 2020 Experiments on probing the configuration space of post-buckled panels. *J. Appl. Mech.* **87**, 121005-1-11. (doi:10.1115/1.4048197)
32. Panter JR, Chen J, Zhang T, Kusumaatmaja H. 2019 Harnessing energy landscape exploration to control the buckling of cylindrical shells. *Commun. Phys.* **2**, 151. (doi:10.1038/s42005-019-0251-4)
33. Evkin A, Krasovsky V, Lykhachova O, Marchenko V. 2019 Local buckling of axially compressed cylindrical shells with different boundary conditions. *Thin-Walled Struct.* **141**, 374–388. (doi:10.1016/j.tws.2019.04.039)
34. Kreilos T, Schneider TM. 2017 Fully localized post-buckling states of cylindrical shells under axial compression. *Proc. R. Soc. A* **473**, 20170177. (doi:10.1098/rspa.2017.0177)
35. Groh RMJ, Pirrera A. 2019 Localised post-buckling states of axially compressed cylinders and their energy barriers. In *AIAA Scitech 2019 Forum, San Diego, CA, 7–11 January*. AIAA 2019-0231.
36. Timoshenko SP, Gere JM. 1963 *Theory of elastic stability*. New York, NY: McGraw-Hill.
37. Hutchinson JW. 2010 Knockdown factors for buckling of cylindrical and spherical shells subject to reduced biaxial membrane stress. *Int. J. Solids Struct.* **47**, 1443–1448. (doi:10.1016/j.ijsolstr.2010.02.009)
38. Hilburger MW. 2018 On the development of shell buckling knockdown factors for stiffened metallic launch vehicle cylinders. In *AIAA/ASCE/AHS/ASC Structures, Structural Dynamics, and Materials Conference, Kissimmee, FL, 8–12 January*. AIAA 2018-1990.
39. Gerasimidis S, Virot E, Hutchinson JW, Rubinstein SM. 2018 On establishing buckling knockdowns for imperfection-sensitive shell structures. *J. Appl. Mech.* **85**, 091010. (doi:10.1115/1.4040455)
40. Mossakovskiy VI, Manevich LI, Evkin AY. 1975 Investigation of post-buckling equilibrium forms of a compressed cylindrical shell. *Prikladnaya Mekhanika* **11**, 1155–1159. (doi:10.1007/BF00883273)
41. Horak J, Lord GJ, Peletier MA. 2006 Cylinder buckling: the mountain pass as an organizing centre. *SIAM J. Appl. Math.* **66**, 1793–1824. (doi:10.1137/050635778)
42. Virgin LN, Wiebe R, Spottswood SM, Eason TG. 2014 Sensitivity in the structural behavior of shallow arches. *Int. J. Nonlin. Mech.* **58**, 212–221. (doi:10.1016/j.ijnonlinmec.2013.10.003)
43. Harvey PS, Virgin LN. 2015 Co-existing equilibria and stability boundaries of a shallow arch: unilateral displacement-control experiments and theory. *Int. J. Solids Struct.* **54**, 1–11. (doi:10.1016/j.ijsolstr.2014.11.016)
44. Cervi C, Santillan ST, Virgin LN. In press Interrogating the configuration space of post-buckled structures. *ASCE J. Eng. Mech*. 149, 04023009. (doi.org/10.1061/JENMDT.EMENG-6839)
45. Ankalhope S, Jose S. 2022 Non-destructive prediction of buckling load of axially compressed cylindrical shells using least resistance path to probing. *Thin-Walled Struct.* **170**, 108497. (doi:10.1016/j.tws.2021.108497)

46. Labans E, Basagni C. 2018 Buckling and free vibration study of variable and constant-stiffness cylindrical shells. *Compos. Struct.* **210**, 446–457. (doi:10.1016/j.compstruct.2018.11.061)
47. Lincoln R, Weaver P, Pirrera A, Groh RM. 2022 Manufacture and buckling test of a variable stiffness, variable thickness composite cylinder under axial compression. In *AIAA SCITECH 2022 Forum, San Diego, CA, 3–7 January*. AIAA-2022-0664.
48. Marthelot J, Jimenez FL, Lee A, Hutchinson JW, Reis PM. 2017 Buckling of a pressurized hemispherical shell subjected to a probing force. *J. Appl. Mech.* **84**, 121005. (doi:10.1115/1.4038063)
49. Harvey PS, Virgin LN. 2015 Effect of stiffener geometry on the behavior of grid-stiffened panels. *ASCE J. Eng. Mech.* **144**, 06017021. (doi:10.1061/(ASCE)EM.1943-7889.0001415)
50. Singer J, Arbocz AJ, Weller T. 2002 *Buckling experiments: experimental methods in buckling of thin-walled structures*, vol. 1 and 2. New York, NY: Wiley.
51. Plaut RH, Virgin LN. 1990 Use of frequency data to predict buckling. *ASCE J. Eng. Mech.* **116**, 2330–2335. (doi:10.1061/(ASCE)0733-9399(1990)116:10(2330))
52. Cooley S, Yang H, Virgin LN. 2023 3D-printing and cylinder buckling: challenges and opportunities. Figshare. (doi:10.6084/m9.figshare.c.6373251)